Journal Pre-proofs

Bilayer biodegradable films prepared by co-extrusion film blowing: mechanical performance, release kinetics of an antimicrobial agent and hydrolytic degradation

Roberto Scaffaro, Andrea Maio, Fortunato E. Gulino, Claudio Di Salvo, Alessia Arcarisi

PII: S1359-835X(20)30074-9
DOI: https://doi.org/10.1016/j.compositesa.2020.105836
Reference: JCOMA 105836

To appear in: *Composites: Part A*

Received Date: 20 November 2019
Revised Date: 13 February 2020
Accepted Date: 16 February 2020

Please cite this article as: Scaffaro, R., Maio, A., Gulino, F.E., Di Salvo, C., Arcarisi, A., Bilayer biodegradable films prepared by co-extrusion film blowing: mechanical performance, release kinetics of an antimicrobial agent and hydrolytic degradation, *Composites: Part A* (2020), doi: https://doi.org/10.1016/j.compositesa.2020.105836

Bilayer biodegradable films prepared by co-extrusion film blowing: mechanical performance, release kinetics of an antimicrobial agent and hydrolytic degradation

Roberto Scaffaro*, Andrea Maio*, Fortunato E. Gulino, Claudio Di Salvo, Alessia Arcarisi

Department of Engineering, University of Palermo, Viale delle Scienze Ed. 6, 90128 Palermo, Italy

* roberto.scaffaro@unipa.it (R.S); andrea.maio@unipa.it (A.M.)

Abstract

Bilayer biodegradable, eco-friendly films were prepared by co-extrusion film blowing, coupling polylactic acid (PLA) and Bio-flex ® (BIO). Furthermore, in the PLA layer, carvacrol (CRV) was added as a natural antimicrobial additive, whereas a nanoclay (D72T) was integrated to protect CRV from volatilization and to modulate release. The materials were analyzed by morphological, chemical-physical, mechanical testing. Furthermore, CRV release and degradation tests were performed. The results pointed out that coupling the two matrices allows gathering the stiffness of PLA with the ductility of BIO. Furthermore, the interlayer adhesion is promoted by CRV. D72T exerts a key-role in avoiding CRV volatilization, thus allowing more prolonged release. Degradation tests results highlight that bilayer films, while being particularly resistant in both acidic and neutral environments, showed a rapid degradation under alkaline conditions, which proved to be intermediate between those of the corresponding monolayers.

Keywords: A. Multifunctional composites; B. Environmental degradation; D. Mechanical testing; E. Extrusion.

1. Introduction

The rising concern toward environmental issues stimulated both academic and industrial efforts in the perspective of reducing packaging waste and, therefore, to replace common polyolefin with compostable or biodegradable bio-sourced polymeric materials [1–3].

In this context, poly(lactic acid) (PLA) is often indicated as the most suitable bio-based polymer material for food packaging applications [4,5]. In fact, it is versatile, compostable, recyclable, and moreover, it possesses high transparency, high molecular weight, high water solubility resistance and good processability [4–7]. Nevertheless, its brittleness or, at least, its scarce ductility may represent shortcomings in packaging application field [8]. The most common strategies adopted to overcome these inconveniences refer to the preparation of polymeric blends with ductile materials or to the use of

plasticizers, as well as the fabrication of multilayer films [5,9–12]. Adding plasticizing agents or blending with other polymers may alter some crucial prerequisites of PLA for food packaging applications, such as non-toxicity, impermeability to O_2 and water, and so on [1,5].

Designing a multi-layer film, on the contrary, enables realizing a multifunctional material, whose characteristics can be optimized and engineered on demand [13,14]. For instance, in the case of food packaging, one can design bilayers constituted by an active layer endowed with antimicrobial properties, intended to be in contact with food, and an external layer acting as a barrier for O_2 and water and/or as a toughening agent, depending on the necessities.

Few papers report on the fabrication of bilayers and, moreover, the assembly of such layers to each other often involves solvent casting or multi-step techniques, which pose several issues in terms of cost-effectiveness and safety from the point of view of human health and environment [1,5,10]. Furthermore, bilayer or, more generally, multilayer films preparation has to face the lack of strong interfacial adhesion, which is typically encountered in most of polymeric systems, which leads to poor ultimate properties [11]. The preparation of bilayers via co-extrusion film blowing represents a key-strategy to avoid time-consuming protocols and toxic solvents, so as to be industrially scalable [1,14]. This technique allows the continuous production of multilayer films involving several operations at the same time: melting, kneading, mixing, stretching, conveying and shaping [1,14]. Indeed, film blowing is currently widespread for industrial production of monolayer packaging films of PLA and other bioplastics, such as Poly(butylene adipate-co-terephthalate) or commercial blends, such as Mater-Bi®, Bioflex® [15–17]. In this context, coupling two different monolayer films of biodegradable polymers can be conveniently used to gather the properties of the two parent components into a unique, novel material. In a previous work, our group demonstrated the possibility to prepare bilayer degradable films based in PLA and Mater-Bi® merging the mechanical robustness of the former and the toughness and stretchability of the latter [1].

Herein, we present the preparation of multilayer films based on biodegradable polymers, namely PLA and Bioflex®, where the PLA-based side, which is intended to stay in contact with food, is loaded with carvacrol as antimicrobial agent and a nanoclay, used for modulating release kinetics and mechanical properties, as well as to inhibit carvacrol volatilization during processing [18]. Bioflex® was used to improve the stretchability of such bilayers, due to its ductility.

2. Materials and methods

2.1 Materials

PLA used was a film grade sample of Ingeo™ Biopolymer 4032D, supplied by NatureWorks (Minnetonka, MN, USA). Bioflex (BIO), trade name Bio-Flex® F2110, was supplied by FKUR (Willich, Germany). It is a sample of a biodegradable polymer blend, whose formulation is proprietary, which contains PLA and a biodegradable co-polyester and some additives [19]. Further information on the structure will be provided in the spectroscopic analysis section.

The main characteristics of the two polymers are listed in **Table 1**.

Table 1. Main properties of raw PLA and BIO used in this work

Main properties	PLA	BIO
Density (g/cm^3)	1.24	1.27
Melting temperature (°C)	155-170	145-160
MFI (g/10 min)	7 [a]	3-5 [b]

[a] at 210 °C and 2.16 kg; [b] at 190 °C and 2.16 Kg

Carvacrol (CRV) essential oil (2-methyl-5-(1-methylethyl)-phenol) was chosen as an antimicrobial agent. CRV, purchased from Sigma Aldrich, has the following specifications: density= 0.9772 g/cm^3, boiling temperature=237.7 ° C, purity ≥97%, and was used as received without further treatments. The nanoclay used was a montmorillonite, modified by dimethyl-dihydrogenated tallow ammonium, Dellite 72T (D72T), supplied by Laviosa Chimica Mineraria, Italy.

2.2 Preparation

2.2.1 Pre-treatment

In order to avoid hydrolytic scission, PLA, BIO and D72T were vacuum-dried in oven prior to processing, adopting the thermal parameters listed in **Table 2**.

Table 2. Parameters adopted for thermal pre-treatment of raw materials

Sample	T (°C)	Time (hours)
PLA	90	14
BIO	90	6
D72T	120	14

For the preparation of PLA-CRV, PLA pellets were preliminary mixed with CRV in a capped flask and mechanically stirred for at least 2 hours in order to achieve total impregnation, while for PLA-CRV-D72T, the dried nanoclay was first impregnated with CRV (1:1) and then stored in a capped flask. The resulting slurry was finally premixed with PLA pellets at the solid state prior to feeding.

2.2.2 Homogenization of the samples via preliminary extrusion

All the materials were homogenized via preliminary extrusion in co-rotating twin-screw extruder (OMC, Italy), adopting the operating parameters listed in **Table 3**. The feeding speed was set at 20 rpm and the extrusion speed was set at 220 rpm, i.e. the maximum operating value that could be set in such equipment, in order to minimize the residence time and, therefore, CRV volatilization. Note that CRV, acting as a plasticizer, decreased the processing temperature of PLA from 190 °C to 170 °C.

Table 3. Operating parameters used for the preliminary extrusion of each material

Sample	CRV wt.%	D72T wt.%	Feeding speed (rpm)	Screw speed (rpm)	T profile (°C)	T_{die} (°C)
PLA	-	-	20	220	160-170-180-190	190
PLA-CRV	5	-	20	220	155-165-165-170	170
PLA-CRV-D72T	5	5	20	220	155-160-165-165	170
BIO	-	-	20	220	120-130-140-150	160

2.2.3 Preparation of monolayer films

The extrudate collected at the end of each extrusion was rapidly cooled in liquid nitrogen to avoid the risk of further volatilization of CRV and pelletized. Monolayer films were prepared via film blowing by using a single-screw extruder, having D=19 mm and L/D=25, equipped with a Brabender film blowing and take-off unit. In particular, PLA-series materials were extruded in a Brabender 832004 (Duisburg, Germany); whereas Bioflex® was processed in a Brabender 814407, (Duisburg, Germania). **Table 4** provides operating parameters and formulations of the monolayer films. Note that thermal profiles selected were the same as those used for the preliminary extrusion in co-rotating twin-screw extruder (see again **Table 3**), while being remarkably lower the screw speed values used, which were optimized to ensure the filmability of each formulation.

Table 4. Operating parameters used for the preparation of monolayer films

Sample	**CRV wt.%***	**D72T wt.%***	Screw speed (rpm)	T profile (°C)	T_{die} (°C)	BUR	Thickness (μm)
PLA	-	-	60	160-170-180-190	190	3.8	22±3
PLA-CRV	5	-	55	155-165-165-170	170	3.8	20±2
PLA-CRV-D72T	5	5	65	155-160-165-165	170	4.3	27±3
BIO	-	-	60	120-130-140-150	160	4	25±4

* based on the total weight of the compounded materials

2.2.4 Fabrication of bilayer films

The bilayer films were prepared by using a co-extrusion blown film line with air cooling equipped with a Brabender film blowing and take-off unit. **Figure 1** provides a pictorial representation of the schematics of the overall process. In particular, PLA and BIO were conveyed into the co-extrusion die allowing to obtain the bilayer tubular film. **Table 5** reports operating conditions adopted in this phase together with blow-up ratio (BUR), calculated as the ratio between the diameters of blown film and die, and film thickness. In this case, it was possible to set the screw speed at 60 rpm for both extruders. Note that the temperature of the film blowing die was kept at 165 °C, i.e. intermediate between those of PLA and BIO. The stability of the bubble during film blowing operation was granted by tuning the air flow rate blown in the bubble and the speed of the take-up rolls. The thickness of the prepared films varied in the range 55–65 µm.

Table 5. Operating parameters used for the preparation of bilayer films prepared

Sample	Screw speeds for both extruders (rpm)	T profile (°C)	T_{die} (°C)	BUR	Thickness (µm)
PLA/BIO	60	PLA 185-200-200-195 BIO 120-130-140-150	165	4.3	57±2
PLA-CRV/BIO	60	PLA 155-165-165-170 BIO 120-130-140-150	165	4.5	58±3
PLA-CRV-D72T/BIO	60	PLA 155-160-165-165 BIO 120-130-140-150	165	3.8	62±3

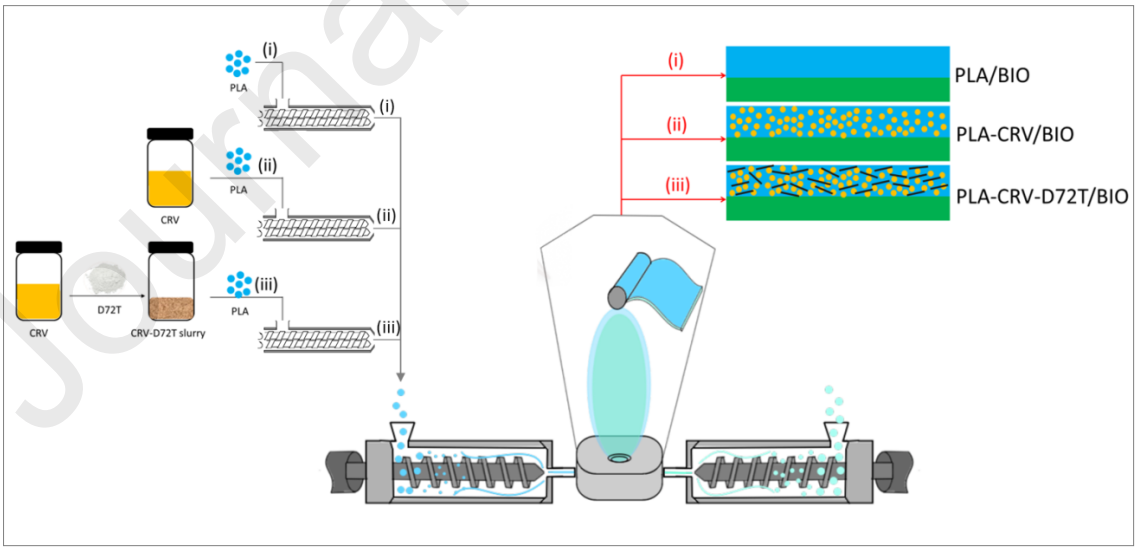

Figure 1. Schematics of the overall process for the preparation of bilayers.

2.3 Characterizations

Morphological analysis was performed by SEM imaging, using an ESEM FEI QUANTA 200 (Thermo Fisher Scientific, USA). In order to inspect the cross-sections of the films, specimens were cryofractured before imaging. Thickness of each layer was measured by Image analysis by means of an open source image processing software (Image J).

Water contact angle (WCA) measurements were carried out at room temperature by using an FTA 1000 (First Ten Ångstroms, UK) instrument. 4 µL of deionized water were dropped onto the surface of each sample by way of an automatic liquid drop dosing system. Images of the drop on the surface were acquired after 20 s.

Tensile tests were performed to evaluate the mechanical properties of the samples, by using an Instron 3365 (Instron, Norwood, MA, USA) universal testing machine, operating at a crosshead speed of 1 mm/min until 3 minutes; thereafter, the crosshead speed was increased to 100 mm/min until specimen failure (ISO 527-3). Elastic modulus (E) was calculated as initial slope of stress-strain curves, extrapolated at zero-strain, tensile strength (TS) and elongation at break were respectively evaluated as the maximum values of stress and strain for each curve. For each experimental run, at least 10 replicates were tested, and the data were provided as mean values with standard deviations.

The structural and chemical composition of each sample were investigated by FTIR-ATR spectroscopy, using a Perkin-Elmer FT-IR/NIR Spectrum 400 spectrophotometer in ATR mode. Spectra, collected in the wavenumber range 4000-400 cm^{-1}, were performed onto both sides of each bilayer. 32 scans were collected for each spectrum, and the measurements were conducted onto at least five replicates for each sample. Moreover, a focus on the range 900-700 cm^{-1} was carried out to qualitatively assess the content of CRV per film unit, since this molecule is characterized by a well-known absorption band at about 814 cm^{-1} [20].

Release of CRV was evaluated by UV-vis spectroscopy, carried out in a UV-vis Specord 252 spectrophotometer (Analytik Jena, Jena, Germany), by monitoring the characteristic signal centered at 273 nm [20]. Spectroscopic data were converted into concentrations by using a calibration line, opportunely constructed according to our previous works [20–22]. The release of CRV was investigated by immersing a pre-weighed sample (a disk with 25 mm diameter) in 10 mL of deionized distilled water (DDW) and thereby monitoring at specific time intervals the absorbance of CRV of the storage solutions until 550 hours. After each measurement, the samples were immersed in fresh DDW to maximize the

diffusion driving force. The cumulative release of CRV was thereby calculated by sequentially adding the amount released after each step.

The degradation tests were carried out by immersing, for each sample, three replicates of disk-shaped specimens, having diameter of 25 mm and thickness of ~60 µm, in three different buffer solutions (pH=4, pH=7 and pH=10) at 37 °C up to 864 hours. At predetermined time intervals, the materials were washed thoroughly with distilled water at room temperature, followed by coagulation in diethyl ether and drying under vacuum in oven for 24 hours. After drying, the samples were weighed and the mass loss was calculated as:

$$M_{loss} = \frac{M_{dry,0} - M_{dry,t}}{M_{dry,0}} \cdot 100 \quad (1)$$

3. Results and discussion

Figs 2 a-c report the SEM micrographs of the cross-sections of PLA/BIO (a), PLA-CRV/BIO (b) and PLA-CRV-D72T/BIO (c) bilayers, together with the thickness of each layer, measured by image analysis.

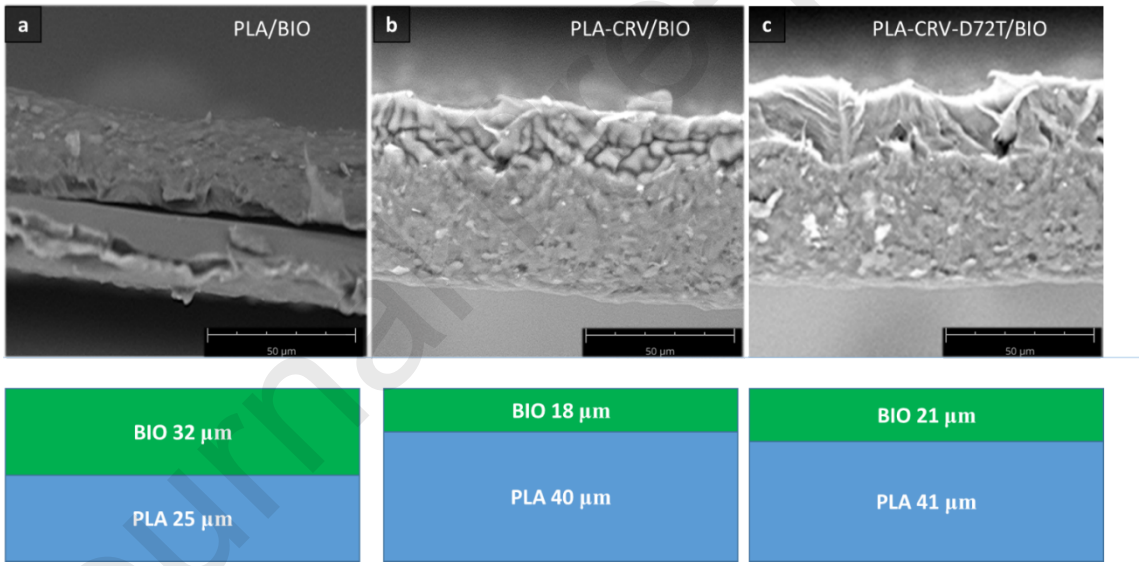

Figure 2. SEM micrographs showing the cross-section of bilayers: (a) PLA/BIO, (b) PLA-CRV/BIO, (c) PLA-CRV-D72T/BIO together with the results of image analysis.

Firstly, the thickness of the two layers was found to be substantially the same in the case of PLA/BIO, Fig. 2a. Differently, adding CRV (Fig. 2b) or CRV+D72T (Fig. 2c) in the PLA-based layer proved to increase the thickness of this latter layer. This aspect can be reasonably explained by taking into account that such bilayers differ each other in terms of both formulation and processing conditions, with obvious repercussions on melt viscosity, BUR, solidification kinetics. Secondly, the interlayer adhesion, which was found to be extremely poor in the case of PLA/BIO, Fig. 2a, proved to dramatically enhance in the

other two formulations, presumably because the presence of CRV promoted surface interactions between the two layers [20,22].

Mechanical properties of the materials prepared in this work are listed in **Table 6**. In the case of monolayer films, PLA and BIO showed mechanical properties consistent with literature data [1,17,23]. As expected, PLA is remarkably stiffer and conversely less deformable than BIO, whose EB proved to be close to 90% (8 times higher than that of PLA). Adding CRV to a PLA led to a decrease of E and TS while slightly enhancing EB. This feature could be reasonably ascribed to the plasticizing effect of CRV. Adding D72T to PLA/CRV resulted in an increase of all the mechanical properties of monolayer films.

Table 6. Mechanical properties derived from tensile tests

Sample	E (MPa)	TS (MPa)	EB (%)
PLA	1800 ± 136	38 ± 2.6	16 ± 5.0
PLA-CRV	1350 ± 80	24 ± 4.0	29 ± 2.1
PLA-CRV-D72T	1500 ± 126	34 ± 3.5	35 ± 1.3
BIO	240 ± 20	8 ± 2.1	92 ± 6.6
PLA/BIO	1500 ± 110	31 ± 3.0	19 ± 4.0
PLA-CRV/BIO	770 ± 60	16 ± 2.6	54 ± 3.4
PLA-CRV-D72T/BIO	1100 ± 103	15 ± 2.2	55 ± 2.8

In the case of bilayer films, instead, the mechanical properties of PLA/BIO proved to be governed by PLA, especially in terms of EB, whereas all the other bilayers prepared in this work showed characteristics intermediate between those of the corresponding monolayers. These findings could be explained by considering the aforementioned differences in terms of interlayer adhesion (see again Figs. 2a-c) and suggest that CRV-aided coupling of two polymers having different behavior via co-extrusion film blowing is a useful strategy in the perspective of fabricating materials with engineered mechanical performance, thereby overcoming the limitations of each starting monolayer. In this context, it is interesting to note that integrating D72T into PLA-CRV allows simultaneously increasing stiffness while retaining or even enhancing stretchability. Such ductility increase is an apparently strange behavior, since it is commonly accepted, except for rare cases [24], that the inclusion of a rigid filler leads to an increase in elastic modulus while being detrimental to EB [25,26]. On the other hand, the presence of nanofillers in systems containing volatile or thermosensitive additives may reduce their volatilization during processing [18,20,27], with the ensuing retention of higher CRV amounts that might have exerted a stronger plasticizing effect. To give further insight into this feature, ATR analysis was performed onto both BIO and PLA-based sides of each bilayer, the spectra are reported in **Figs 3 a-b**. Note that spectra collected on BIO side proved to be unaltered, hence only one spectrum was reported in the plot. It is

worth highlighting that no differences were detected between the spectrum of BIO monolayer film and the spectra of bilayers performed onto BIO side, as well as between the spectra of PLA-based monolayers and those of PLA side in bilayers, thus suggesting that the two polymers did not mix each other during the fabrication of the bilayer films.

PLA spectrum shows the typical bands reported elsewhere: in detail, a weak band located at 3500 cm^{-1} is traditionally ascribed to –OH stretching, the modes centered at 2997 cm^{-1}, 2946 cm^{-1}, 1456 cm^{-1} and 1382 cm^{-1} are attributed to $–CH_3$ stretching, the band at 1748 cm^{-1} refers to C=O stretching, the signal at 1225 cm^{-1} is ascribed to C=O bending, those centered at 1194, 1130, 1093 cm^{-1} are due to –C–O– stretching, the band at 1047 cm^{-1} is related to –OH bending; those located at 956 and 921 cm^{-1} are ascribed to $–CH_3$ rocking; finally, those centered at 926 cm^{-1} and 868 cm^{-1} are attributed to C–C– stretching [1,20,22,28,29]. The results of spectroscopic analysis are fully consistent with the hypothesized composition of this material.

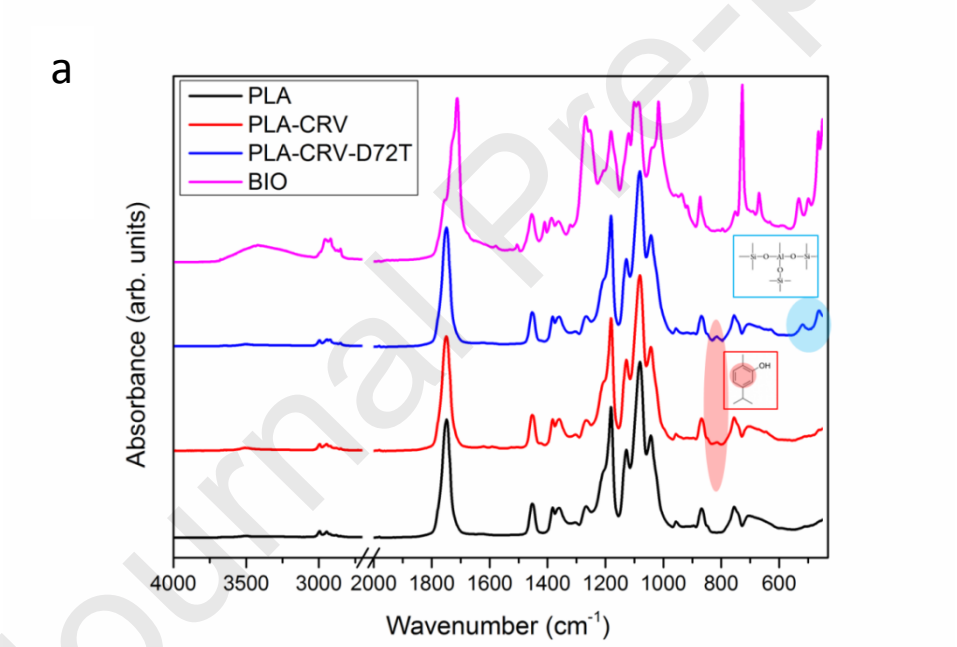

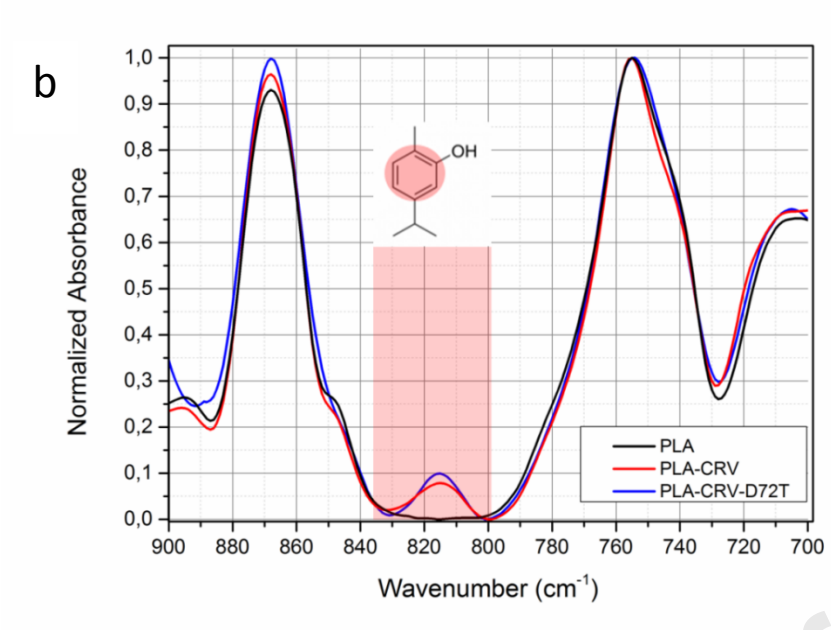

Figure 3. (a) FTIR/ATR spectra collected in the range 4000-450 cm^{-1} onto BIO-based side and PLA-based side for the bilayers prepared; (b) close-up of the spectral range 900-700 cm^{-1} useful for the detection of CRV collected for PLA-based side of each bilayer, normalized to the intensity of the band centered at 740 cm^{-1}.

As pointed out in the experimental part, BIO is a polymeric material whose formulation is proprietary. However, the analysis of ATR spectrum, put into evidence the presence of well-known absorption modes: a broad and relatively very intense band at 3600-3000 cm^{-1} suggests the presence of OH-moieties, bands located at 2957 and 2864 cm^{-1} are typically due to C-H stretching of $–CH_3$ moieties, a band at 1712 cm^{-1} can be assigned to C=O stretching, the absorption band at 1455 cm^{-1} may refer to scissoring of $–CH_2$ groups, while the modes centered at 1412 cm^{-1} and 1378 cm^{-1} can be ascribed to C-H rocking. Furthermore, those centered at 1273, 1163, 1117 and 1104 cm^{-1} are attributed to C-O stretching, while those located at 1016, 931, 867 and 729 cm^{-1} refer to C-H bending [30–33]. The presence of CRV in PLA-CRV and PLA-CRV-D72T can be detected by monitoring the signal centered at 811 cm^{-1} due to aromatic ring of CRV [20–22]. Furthermore, in the case of PLA-CRV-D72T, the successful integration of nanoclays into polymeric matrix are confirmed by the insurgence of bands in the spectral range 550-500 cm^{-1}, ascribed to $-Al_2Si_2O_5(OH)_4$, otherwise not detected [34].

Aiming to evaluate the amount of CRV entrapped in the films, the spectral region 900-700 cm^{-1} of the spectra is provided in the panel b of the same figure. Spectra were normalized with respect to that centered at 753 cm^{-1} which proved to be unaltered for all the samples [20,22]. The result highlighted that CRV signal in PLA-CRV-D72T has an intensity 25% higher than that of PLA-CRV. This feature may suggest that CRV amount is higher when D72T is used.

The amount of CRV released per 100 mg of film is provided in **Figure 4**.

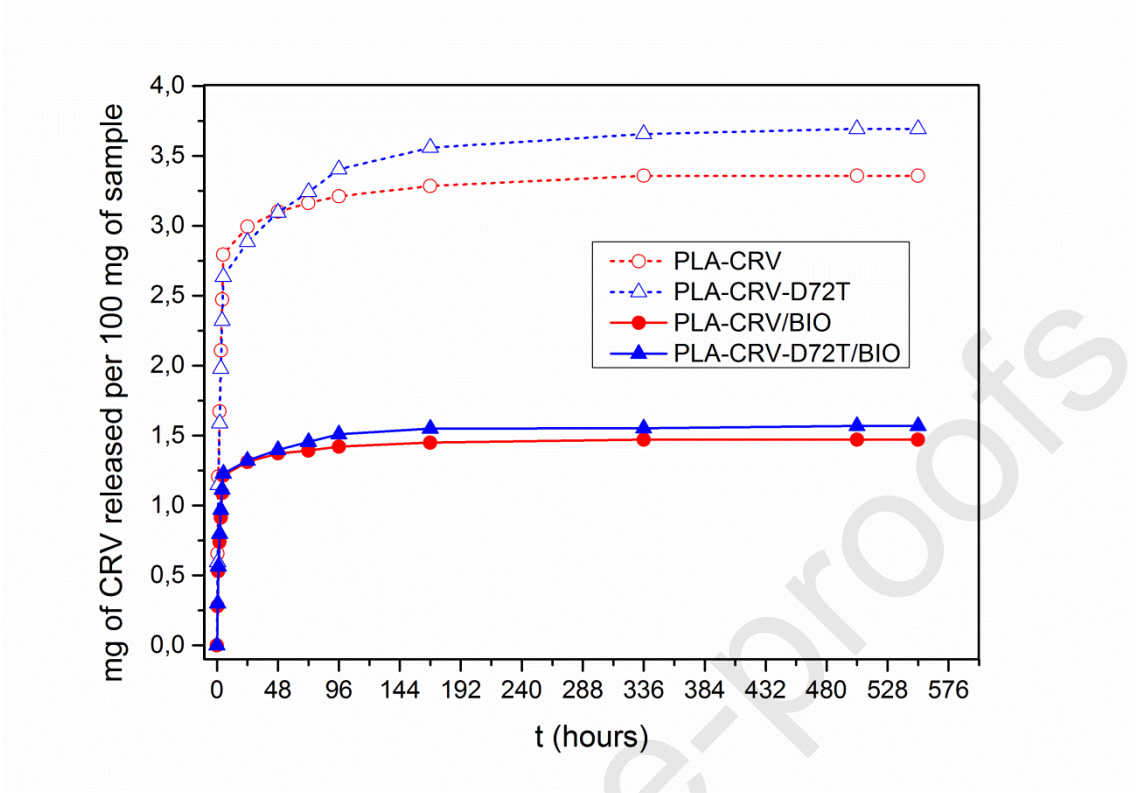

Figure 4. Release tests: amount of CRV released per 100 mg film.

All the materials showed a burst release at the early stages of the experiment, followed by a plateau, while differing each other for the amount of CRV released at plateau, depending on formulation and structure. Of course, being CRV contained only in PLA-side, monolayers possess an overall concentration of CRV higher than bilayers. Furthermore, in monolayers the CRV molecules may diffuse out from both sides of the film specimen, whereas in the case of bilayer, only PLA-based side is exposed to aqueous medium, while the other is capped by the presence of BIO layer. For these reasons, the final amount of CRV released at the end of experiment is found to vary consequently.

Notably, in both monolayers and bilayers, the materials containing D72T display highest amount of CRV released, likely due to the highest loading efficiency, as confirmed by ATR analysis. Beyond the clear differences observed in terms of final amount of CRV released, some differences in release kinetics can be envisaged. In fact, it is possible to detect intersections between the curves of PLA-CRV and PLA-CRV-D72T monolayers, as well as between those of the corresponding bilayers. Aiming to study the kinetics of such release behaviors, the amounts of CRV released upon immersion time were normalized to those released at the end of experiment, i.e. the maximum values, and reported in **Figure 5**.

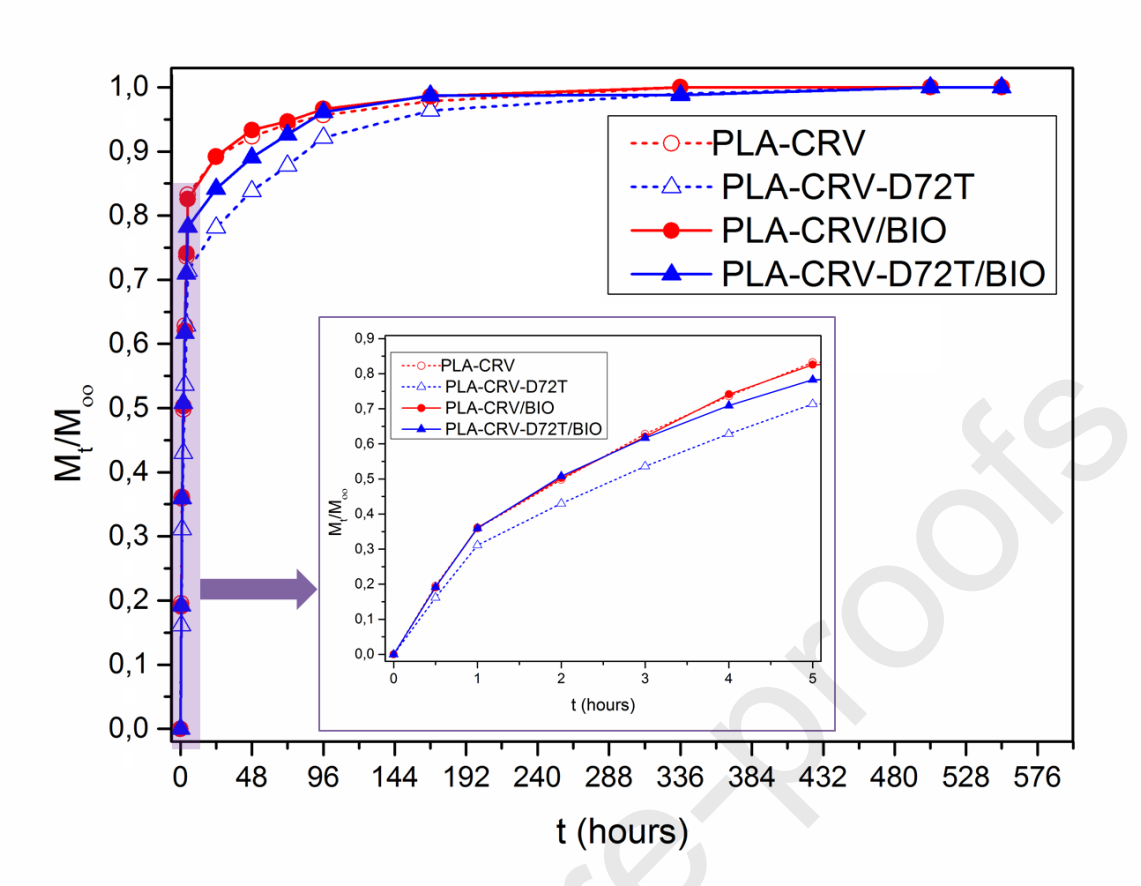

Figure 5. Normalized cumulative CRV release as a function of time from the samples investigated. Inset: early portion of the release curves to highlight the burst region.

The results highlighted that no significant difference was detected among PLA-CRV, PLA-CRV/BIO and PLA-CRV-D72T/BIO during the burst phase, whereas PLA-CRV-D72T showed a slower release. Thereafter, the formulations containing D72T displayed kinetics delivery slower than those without nanoclay.

In order to perform a closer inspection of release mechanism, experimental data were fitted according to Peppas-Korsmeyer model [35–38]:

$$\frac{M_t}{M_\infty} = kt^n \qquad (2)$$

Where t is the release time, k is a kinetic constant related to the properties of the drug delivery system, and n is the diffusion exponent that is an indicator about the release mechanism.

M_∞ is the mass delivered at the depletion time, usually calculated as the value of cumulative mass released at saturation [27,39,40]. In this case, all the samples came to depletion, since in all cases a well-

defined plateau was achieved. In PLA-CRV and PLA-CRV/BIO systems, CRV was no longer released after 336 hours; for the systems containing D72T, instead, no CRV release was observed after 504 hours.

Figure 6 provides log M_t/M_∞ plotted as a function of log time for each sample. The release data were fitted by using Equation (1) until a satisfactory R^2 value (>0.99) was achieved [41]. It is worth noting that Peppas-Korsmeyer model is applicable only in the early portion of each curve, that is for $M_t/M_\infty<0.6$ [42]. Therefore, by analysing the slope and the intercept of the fitted lines in the first interval, it is possible to calculate n and k, respectively. The physical meaning of *n* is related to the release mechanism. In fact, when n≤0.5 (Case I), the drug release is dominated by diffusive phenomena. In this case, the solvent transport rate is higher than the polymer chains relaxation. Equilibrium of absorption in the surface exposed of the system is rapidly achieved, thus leading to a time-dependent drug release. Note that when n=0.5, Equation (1) coincides with the Fick's law [43]. Case I is usually exhibited by rigid, hydrophobic matrices. Whether n=1 (Case II), drug release is governed by swelling or relaxation phenomena, and a zero-order release kinetics is observed. This situation usually refers to swellable matrices. Values of n between 0.5 and 1.0 indicate an anomalous transport, resulting from the combination of both diffusive and swelling phenomena. In this case, the diffusion and swelling rates are comparable, thus simultaneously giving rise to the time-dependent anomalous effects [43]. Finally, n>1 indicates a Super Case II transport, triggered by erosive phenomena that enable an extremely fast drug release. This phenomenon occurs when matrices used for delivery systems are subjected to erosive phenomena that enable an extremely fast drug release. **Figure 6** put into evidence that all the materials prepared in this work follow the same burst release mechanism, characterized by an initial anomalous release (n~0.9) in the early region, followed by a diffusion-driven release, with n values close to 0.5 (see evidenced zones in the plot of Fig. 6). At the initial stage, the release of CRV may depend on superficial availability of CRV molecules that can rapidly leave the polymeric structure and on swelling behavior of polymer matrix [27,39].

This aspect was investigated by performing WCA measurements, whose results are shown in **Table 7**. All the films displayed WCA less than 90° and those containing CRV displayed surface wettability moderately higher than PLA and BIO. This feature, together with the higher stretchability of materials containing CRV, leads to slightly easier penetration of the solvent, which cooperates with diffusion of CRV molecules.

Table 7. WCA results

Sample	WCA (°)
PLA	72.8 ± 0.4
PLA-CRV	66.6 ± 0.8
PLA-CRV-D72T	62.7 ± 1.2
BIO	67.8 ± 0.9
PLA/BIO	72.8 ± 0.4 (PLA side) 67.8 ± 0.9 (BIO side)
PLA-CRV/BIO	66.8 ± 1.0 (PLA-CRV side) 67.8 ± 0.7 (BIO side)
PLA-CRV-D72T/BIO	62.7 ± 1.0 (PLA-CRV-D72T side) 67.8 ± 0.7 (BIO side)

However, as previously observed, the strongest differences in terms of release kinetics were observed after 3-4 hours, when tortuosity imparted by nanoclays structured throughout the polymer matrix made more difficult for CRV molecules to leave the structure and, probably, the presence of a rigid filler restrained the macromolecules relaxation, thus decreasing the swelling behavior of the matrix.

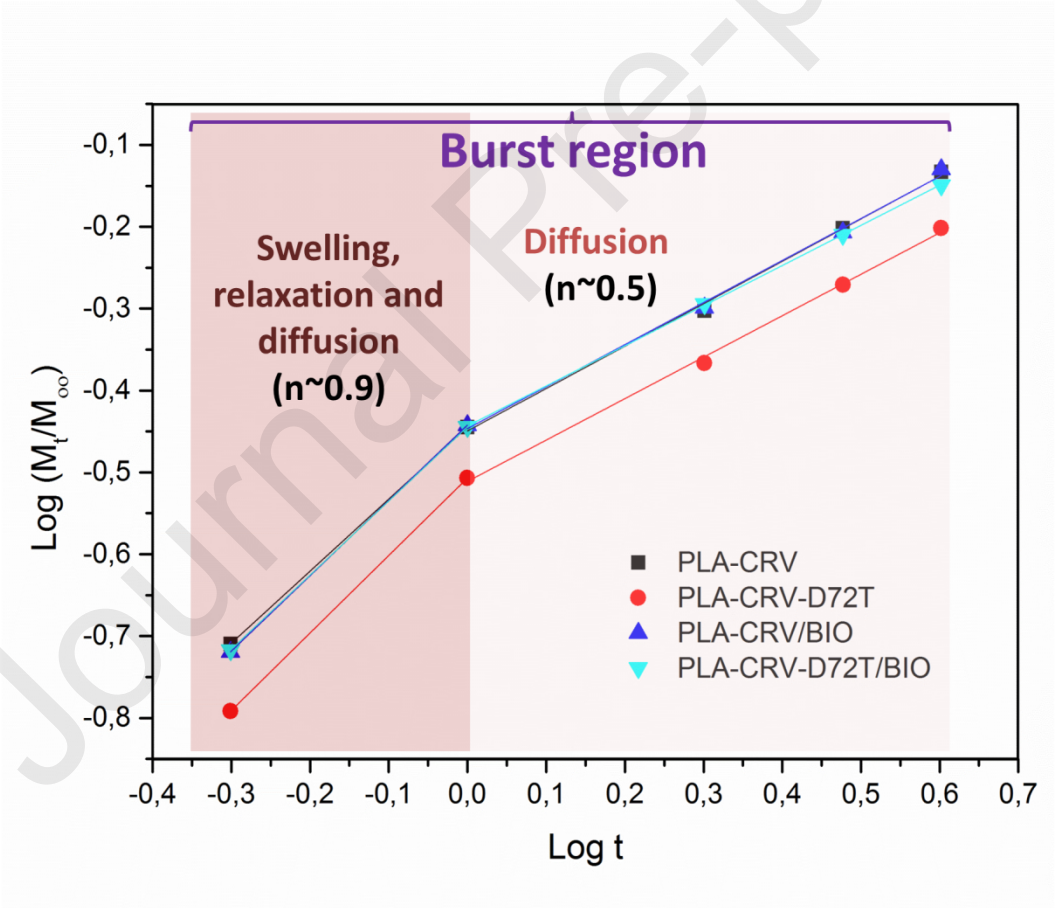

Figure 6. Power law model applied to the release data achieved during Burst release region

It is worth highlighting that all the formulations tested proved to display excellent resistance at pH=4 and pH=7, since no appreciable changes was detected after 864 hours immersion [44]. For this reason, only

the results of hydrolytic degradation tests performed at pH=10 are provided in **Figure 7**, where the evolution of mass loss curves is reported as a function of immersion time (t).

The analysis of such curves pointed out that degradation behaviour of PLA-series monolayers is much different from that of BIO and bilayers. In fact, after 288 hours, the former class of materials proved to be totally degraded, while BIO was found to retain more than 90% of its initial mass. This latter occurrence can be likely ascribed to the different formulation of this resin and/or to the eventual presence of natural stabilizers, among the additives declared by manufacturer.

Among PLA-series monolayers, inclusion of CRV and D72T determined slight differences in kinetics of hydrolytic reactions, which however were found to be faster than those of neat PLA. This issue can be reasonably ascribed to higher hydrophilicity of materials containing CRV with respect to PLA. All the bilayer films displayed mass loss values intermediate between those of the corresponding monolayers. However, an opposite trend was found. Differently from what seen in the case of monolayer films, PLA/BIO bilayer showed a degradation faster than those of PLA-CRV/BIO and PLA-CRV-D72T/BIO. This apparently strange behavior was ascribed to delamination phenomena detected for PLA/BIO, which were suppressed in the materials containing CRV, owing to a stronger interlayer adhesion [1].

At the end of the experiment, while PLA-series monolayers displayed a total mass loss, BIO monolayer lost only 40% of its initial mass. For PLA/BIO, PLA-CRV/BIO and PLA-CRV-D72T/BIO the mass loss values were respectively: 70%, 56% and 55%.

Actually, according to the scientific literature [45,46], the typical degradation kinetics, for systems with mass loss curves exhibiting positive concavity (i.e. with progressive increase of degradation kinetics) can be modeled by means of exponential functions like those reported in Eqns. 3-4

$$M_{loss} = A_2 + \frac{A_1 - A_2}{1 - \exp\left[(t - t_0)/\tau\right]} \qquad (3)$$

$$M_{loss} = \begin{cases} 1 - \exp\left(-k_1 t\right) & (4) \\ 1 - \exp\left[-(k_1 + k_2)t\right] & (5) \end{cases}$$

In Eqn. 3, describing systems with complete/bulk autocatalytic degradation, A_1 and A_2 are parameters taking into account initial and final conditions, t_0 is the center of the sigmoid (i.e. the time at which mass loss is the half of its maximum value) and τ is a time constant.

In Eqns. 4-5, describing systems with non-complete autocatalytic degradation, k_1 and k_2 indicate the rate constants associated to, respectively, surface degradation stage and degradation penetration stage [46].

It is worth noting that PLA monolayer series finds best fitting using Eqn. 3, while BIO bilayer series finds best fitting using Eqns. 4-5.

In tables 8-9, there are reported the best fitting results for, respectively, PLA and BIO materials series.

It can be observed that both R^2 (>0.99) and χ^2 (0.05) values are more than satisfactory.

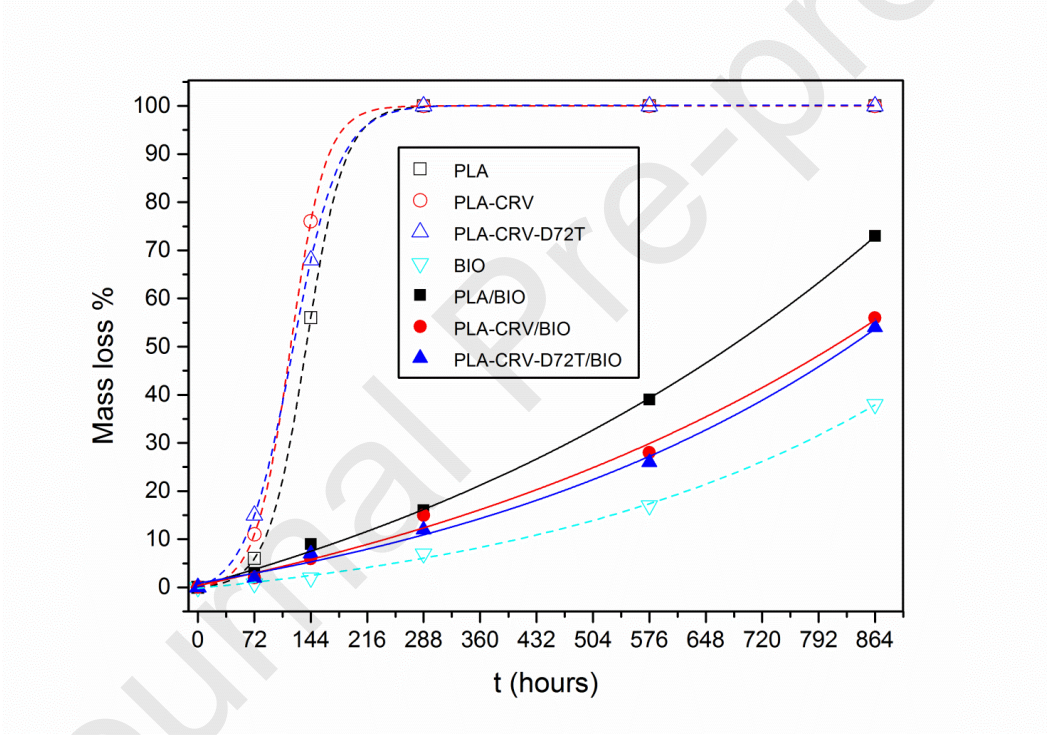

Figure 7. Degradation tests at pH=10: mass loss as a function of immersion time, fitted by Eq. 3.

Table 8. Fitting results of experimental data of PLA-series materials, provided in Fig.7.

Sample	A_1	A_2	t_0	τ	R^2	χ^2
PLA	-0.345	100.072	137.988	24.455	0.99999	0.01584
PLA-CRV	-0.526	100.017	117.951	22.478	1	9.94E-4
PLA-CRV-D72T	-1.774	100.125	120.729	29.978	0.99998	0.04921

Table 9. Fitting results of BIO and bilayers, according to Eqs. (4-5)

Sample	k_1 (h^{-1})	k_2 (h^{-1})	R^2*
BIO	2.9892E-4	0.0007	0.990
PLA/BIO	6.0615E-4	0.0022	0.993
PLA-CRV/BIO	5.5916E-4	0.0011	0.993
PLA-CRV-D72T/BIO	5.0417E-4	0.0012	0.993

(*) referred to Eqn.4 first stage fitting. Eqn. 5 was applied to two points only

The analysis of k_1 and k_2 values, listed in Tab. 9, confirms the low degradation kinetics in both stages in BIO and a higher degradation rate when PLA is present, according to the faster degradation kinetics of PLA monolayers commented above. The highest degradation rate of PLA/BIO systems can be reasonably ascribed to the aforementioned delamination phenomena.

4. Conclusions

The results herein presented show that it is possible achieving bilayer films containing an essential oil, CRV, by co-extrusion film blowing, continuously in the melt, without using toxic solvents or time-consuming protocols. Adding CRV to PLA imparted significant modifications to processing, structure and ultimate properties of such films. CRV proved to act as a plasticizer, thus enabling to process PLA at lower temperatures, and it was found to improve interlayer adhesion in PLA-BIO bilayers and ductility of such films. Conversely, the tendency of CRV to volatilize may pose some problems in terms of loading efficiency and too much rapid depletion times of the systems. Aiming to overcome or modulate these issues, the further incorporation of a nanoclay sample, D72T, was successfully tested. D72T, beyond the obvious advantages in terms of mechanical properties, proved to protect CRV from volatilization, thus increasing CRV loading efficiency into PLA matrix, while allowing a slower release kinetics that resulted in a more prolonged release of antimicrobial additive.

Degradation tests at different pH values, pointed out that all bilayers and monolayers displayed a remarkable stability when exposed to acidic and neutral environment, while being rapidly degraded in alkaline conditions. PLA-based monolayers displayed a total mass loss within about 250 hours, whereas BIO showed a stronger resistance. Bilayers exhibited a behavior intermediate between those of the corresponding monolayers.

References

[1] Scaffaro R, Sutera F, Botta L. Biopolymeric bilayer films produced by co-extrusion film blowing. Polym Test 2018;65:35–43. doi:https://doi.org/10.1016/j.polymertesting.2017.11.010.

[2] Bourtoom T, Chinnan MS. Preparation and properties of rice starch-chitosan blend biodegradable film. LWT - Food Sci Technol 2008;41:1633–41. doi:10.1016/j.lwt.2007.10.014.

[3] Claro PIC, Neto ARS, Bibbo ACC, Mattoso LHC, Bastos MSR, Marconcini JM. Biodegradable blends with potential use in packaging: a comparison of PLA/Chitosan and PLA/Cellulose Acetate films. J Polym Environ 2016;24:363–71. doi:10.1007/s10924-016-0785-4.

[4] Sanyang ML, Sapuan SM. Development of expert system for biobased polymer material selection: food packaging application. J Food Sci Technol 2015;52:6445–54. doi:https://doi.org/10.1007/s13197-015-1759-6.

[5] Scaffaro R, Maio A, Sutera F, Gulino EF, Morreale M. Degradation and recycling of films based on biodegradable polymers: a short review. Polymers (Basel) 2019;11:651. doi:10.3390/polym11040651.

[6] Scaffaro R, Maio A, Lo Re G, Parisi A, Busacca A. Advanced piezoresistive sensor achieved by amphiphilic nanointerfaces of graphene oxide and biodegradable polymer blends. Compos Sci Technol 2018;156:166–76. doi:https://doi.org/10.1016/j.compscitech.2018.01.008.

[7] Scaffaro R, Maio A. Integrated ternary bionanocomposites with superior mechanical performance via the synergistic role of graphene and plasma treated carbon nanotubes. Compos Part B Eng 2019. doi:https://doi.org/10.1016/j.compositesb.2019.03.076.

[8] Gupta A, Simmons W, Schueneman GT, Hylton D, Mintz EA. Rheological and thermo-mechanical properties of poly(lactic acid)/lignin-coated cellulose nanocrystal composites. ACS Sustain Chem Eng 2017;5:1711–20. doi:10.1021/acssuschemeng.6b02458.

[9] Al-Itry R, Lamnawar K, Maazouz A. Improvement of thermal stability, rheological and mechanical properties of PLA, PBAT and their blends by reactive extrusion with functionalized epoxy. Polym Degrad Stab 2012;97:1898–914.

[10] Altan A, Aytac Z, Uyar T. Carvacrol loaded electrospun fibrous films from zein and poly(lactic acid) for active food packaging. Food Hydrocoll 2018;81:48–59. doi:https://doi.org/10.1016/j.foodhyd.2018.02.028.

[11] Sanyang ML, Sapuan SM, Jawaid M, Ishak MR, Sahari J. Development and characterization of sugar palm starch and poly (lactic acid) bilayer films. Carbohydr Polym 2016;146:36–45.

[12] González A, Alvarez Igarzabal CI. Soy protein - Poly (lactic acid) bilayer films as biodegradable material for active food packaging. Food Hydrocoll 2013;33:289–96. doi:10.1016/j.foodhyd.2013.03.010.

[13] Scaffaro R, Lopresti F, Maio A, Sutera F, Botta L. Development of polymeric functionally graded scaffold: a brief review. J Appl Biomater Funct Mater 2016;In Press. doi:10.5301/jabfm.5000252.

[14] Botta L, Scaffaro R, Sutera F. Biopolymeric bilayer films for packaging applications prepared by co-extrusion film blowing. J. Appl. Biomater. Funct. Mater., vol. 15, 2017, p. e409--e410. doi:10.5301/jabfm.5000369.

[15] Arruda LC, Magaton M, Bretas RES, Ueki MM. Influence of chain extender on mechanical, thermal and morphological properties of blown films of PLA/PBAT blends. Polym Test 2015;43:27–37. doi:https://doi.org/10.1016/j.polymertesting.2015.02.005.

[16] Briassoulis D, Giannoulis A. Evaluation of the functionality of bio-based food packaging films. Polym Test 2018;69:39–51. doi:https://doi.org/10.1016/j.polymertesting.2018.05.003.

[17] La Mantia FP, Ceraulo M, Mistretta MC, Morreale M. Rheological behaviour, mechanical properties and processability of biodegradable polymer systems for film blowing. J Polym Environ 2018;26:749–55. doi:10.1007/s10924-017-0995-4.

[18] Yang C, Tang H, Wang Y, Liu Y, Wang J, Shi W, et al. Development of PLA-PBSA based biodegradable active film and its application to salmon slices. Food Packag Shelf Life

2019;22:100393. doi:https://doi.org/10.1016/j.ipsi.2019.100393.

[19] Gregorova A, Riedl E, Sedlarik V, Stelzer F. Effect of 4,4′-methylenediphenyl diisocyanate on thermal and mechanical properties of Bioflex/lactic acid polycondensate blends. Asia-Pacific J Chem Eng 2012;7:S317–23. doi:10.1002/apj.1650.

[20] Scaffaro R, Maio A, Lopresti F. Effect of graphene and fabrication technique on the release kinetics of carvacrol from polylactic acid. Compos Sci Technol 2019;169. doi:10.1016/j.compscitech.2018.11.003.

[21] Scaffaro R, Lopresti F, D'Arrigo M, Marino A, Nostro A. Efficacy of poly(lactic acid)/carvacrol electrospun membranes against Staphylococcus aureus and Candida albicans in single and mixed cultures. Appl Microbiol Biotechnol 2018;102:4171–81. doi:10.1007/s00253-018-8879-7.

[22] Scaffaro R, Lopresti F. Processing, structure, property relationships and release kinetics of electrospun PLA/Carvacrol membranes. Eur Polym J 2018;100:165–71. doi:10.1016/j.eurpolymj.2018.01.035.

[23] Scaffaro R, Botta L, Maio A, Mistretta MC, La Mantia FP. Effect of graphene nanoplatelets on the physical and antimicrobial properties of biopolymer-based nanocomposites. Materials (Basel) 2016;9. doi:10.3390/ma9050351.

[24] Scaffaro R, Maio A. Influence of oxidation level of graphene oxide on the mechanical performance and photo-oxidation resistance of a polyamide 6. Polymers (Basel) 2019;11:857. doi:10.3390/polym11050857.

[25] Maio A, Fucarino R, Khatibi R, Rosselli S, Bruno M, Scaffaro R. A novel approach to prevent graphene oxide re-aggregation during the melt compounding with polymers. Compos Sci Technol 2015;119:131–7. doi:http://dx.doi.org/10.1016/j.compscitech.2015.10.006.

[26] Scaffaro R, Maio A. Optimization of two-step techniques engineered for the preparation of polyamide 6 graphene oxide nanocomposites. Compos Part B Eng 2019;165:55–64. doi:10.1016/j.compositesb.2018.11.107.

[27] Scaffaro R, Maio A, Nostro A. Poly(lactic acid)/carvacrol-based materials: preparation, physicochemical properties, and antimicrobial activity. Appl Microbiol Biotechnol 2020. doi:10.1007/s00253-019-10337-9.

[28] Kister G, Cassanas G, Vert M. Effects of morphology, conformation and configuration on the IR and Raman spectra of various poly(lactic acid)s. Polymer (Guildf) 1998;39:267–73. doi:https://doi.org/10.1016/S0032-3861(97)00229-2.

[29] Davis EM, Theryo G, Hillmyer MA, Cairncross RA, Elabd YA. Liquid Water Transport in Polylactide Homo and Graft Copolymers. ACS Appl Mater Interfaces 2011;3:3997–4006. doi:10.1021/am2008618.

[30] Maio A, Giallombardo D, Scaffaro R, Palumbo Piccionello A, Pibiri I. Synthesis of a fluorinated graphene oxide--silica nanohybrid: improving oxygen affinity. RSC Adv 2016;6:46037–47. doi:10.1039/c6ra02585d.

[31] Maio A, Scaffaro R, Lentini L, Palumbo Piccionello A, Pibiri I. Perfluorocarbons–graphene oxide nanoplatforms as biocompatible oxygen reservoirs. Chem Eng J 2018;334:54–65. doi:10.1016/j.cej.2017.10.032.

[32] Scaffaro R, Maio A, Lopresti F, Giallombardo D, Botta L, Bondì ML, et al. Synthesis and self-assembly of a PEGylated-graphene aerogel. Compos Sci Technol 2016;128. doi:10.1016/j.compscitech.2016.03.030.

[33] Rapisarda M, La Mantia FP, Ceraulo M, Mistretta MC, Giuffrè C, Pellegrino R, et al. Photo-oxidative and soil burial degradation of irrigation tubes based on biodegradable polymer blends. Polymers (Basel) 2019;11. doi:10.3390/polym11091489.

[34] De Maria A, Aurora A, Montone A, Tapfer L, Pesce E, Balboni R, et al. Synthesis and characterization of PMMA/silylated MMTs. J Nanoparticle Res 2011;13:6049–58. doi:10.1007/s11051-011-0496-7.

[35] Scaffaro R, Botta L, Maio A, Mistretta MC, La Mantia FP. Effect of Graphene Nanoplatelets on the Physical and Antimicrobial Properties of Biopolymer-Based Nanocomposites. Materials

(Basel) 2016;9:351. doi:10.3390/ma9050351.

[36] Saha NR, Sarkar G, Roy I, Rana D, Bhattacharyya A, Adhikari A, et al. Studies on methylcellulose/pectin/montmorillonite nanocomposite films and their application possibilities. Carbohydr Polym 2016;136:1218–27. doi:https://doi.org/10.1016/j.carbpol.2015.10.046.

[37] Keawchaoon L, Yoksan R. Preparation, characterization and in vitro release study of carvacrol-loaded chitosan nanoparticles. Colloids Surfaces B Biointerfaces 2011;84:163–71. doi:https://doi.org/10.1016/j.colsurfb.2010.12.031.

[38] Ritger PL, Peppas NA. A simple equation for description of solute release II. Fickian and anomalous release from swellable devices. J Control Release 1987;5:37–42.

[39] Scaffaro R, Maio A, Gulino EF, Micale GDM. PLA-based functionally graded laminates for tunable controlled release of carvacrol obtained by combining electrospinning with solvent casting. React Funct Polym 2020:104490. doi:https://doi.org/10.1016/j.reactfunctpolym.2020.104490.

[40] Scaffaro R, Maio A, Lopresti F. Effect of graphene and fabrication technique on the release kinetics of carvacrol from polylactic acid. Compos Sci Technol 2019;169:60–9. doi:https://doi.org/10.1016/j.compscitech.2018.11.003.

[41] Scaffaro R, Maio A, Botta L, Gulino EF, Gulli D. Tunable release of Chlorhexidine from Polycaprolactone-based filaments containing graphene nanoplatelets. Eur Polym J 2019;110:221–32. doi:10.1016/j.eurpolymj.2018.11.031.

[42] Dias MV, Sousa MM, Lara BRB, de Azevedo VM, de Fátima Ferreira Soares N, Borges SV, et al. Thermal and morphological properties and kinetics of diffusion of antimicrobial films on food and a simulant. Food Packag Shelf Life 2018;16:15–22. doi:https://doi.org/10.1016/j.fpsl.2018.01.007.

[43] Bruschi ML. Strategies to Modify the Drug Release from Pharmaceutical Systems. 2015. doi:10.1016/C2014-0-02342-8.

[44] Scaffaro R, Maio A, Gulino EF, Pitarresi G. Lignocellulosic fillers and graphene nanoplatelets as hybrid reinforcement for polylactic acid: Effect on mechanical properties and degradability. Compos Sci Technol 2020:108008. doi:https://doi.org/10.1016/j.compscitech.2020.108008.

[45] Wan L, Li C, Sun C, Zhou S, Zhang Y. Conceiving a feasible degradation model of polylactic acid-based composites through hydrolysis study to polylactic acid/wood flour/polymethyl methacrylate. Compos Sci Technol 2019;181. doi:10.1016/j.compscitech.2019.06.002.

[46] Vey E, Rodger C, Meehan L, Booth J, Claybourn M, Miller AF, et al. The impact of chemical composition on the degradation kinetics of poly(lactic-co-glycolic) acid copolymers cast films in phosphate buffer solution. Polym Degrad Stab 2012;97:358–65. doi:https://doi.org/10.1016/j.polymdegradstab.2011.12.010.

Declaration of interests

☒ The authors declare that they have no known competing financial interests or personal relationships that could have appeared to influence the work reported in this paper.

☐The authors declare the following financial interests/personal relationships which may be considered as potential competing interests:

Roberto Scafaro: Conceptualization, Methodology, Supervision, Formal Analysis, Data Curation, Writing-Reviewing and Editing, Resources, Project administration.

Andrea Maio: Conceptualization, Investigation, Methodology, Formal analysis, Software, Visualization, Data Curation, Writing-Reviewing and Editing, Writing-Original draft preparation.

Emmanuel F Gulino: Investigation, Visualization, Data Curation, Software.

Claudio Di Salvo: Investigation, Data Curation.

Alessia Arcarisi: Investigation.